

Article

Synergetic Impact of Secondary Metal Oxides of Cr-M/MCM41 Catalyst Nanoparticles for Ethane Oxidative Dehydrogenation Using Carbon Dioxide

Abdulrhman S. Al-Awadi ¹, Ahmed Mohamed El-Toni ^{2,3,*}, Mansour Alhoshan ¹,
Aslam Khan ² , Muhammad Ali Shar ² , Ahmed E. Abasaheed ¹  and Saeed M. Al-Zahrani ¹

¹ Chemical Engineering Department, King Saud University, Riyadh 11421, Saudi Arabia; alawadi@KSU.EDU.SA (A.S.A.-A.); mhoshan@KSU.EDU.SA (M.A.); abasaheed@KSU.EDU.SA (A.E.A.); szahrani@ksu.edu.sa (S.M.A.-Z.)

² King Abdullah Institute for Nanotechnology, King Saud University, Riyadh 11451, Saudi Arabia; aslamkhan@ksu.edu.sa (A.K.); mashar@ksu.edu.sa (M.A.S.)

³ Central Metallurgical Research and Development Institute, CMRDI, Helwan 11421, Egypt

* Correspondence: aamohammad@ksu.edu.sa

Received: 26 November 2019; Accepted: 11 December 2019; Published: 20 December 2019

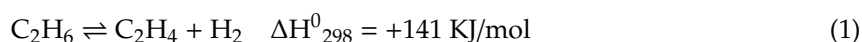


Abstract: Oxidative dehydrogenation of alkanes to alkenes by a mild oxidant such as carbon dioxide is an active area of research. A series of MCM41-supported bimetallic oxide catalysts containing chromium oxide in addition to metal oxides (Ce, Co, Zn, V, Nb, and Mo) has been prepared. The binary catalysts have Cr metal oxide incorporated into MCM41 structure while the other oxides are either incorporated with Cr or impregnated on the MCM41 surface. The synthesized catalysts were characterized by X-ray diffraction (XRD), transmission electron microscopy (TEM), N₂ sorption, scanning electron microscopy (SEM), hydrogen temperature programmed reduction (H₂-TPR), and Diffuse reflectance UV–vis spectroscopy (DRS). The catalytic activity of Cr(4)-M(4)/MCM-41 catalysts in the dehydrogenation of ethane with CO₂ was investigated. The textural properties of the synthesized samples showed that the addition of the bimetallic oxides did not disturb the mesoporous structure of MCM41 and the prepared catalysts exhibited a high BET surface area; however, the lowest surface area was recorded for Cr(4)-Mo(4)/MCM41 catalyst at 701 m²/g. Among the prepared catalysts, H₂-TPR profile of Cr(4)-Ce(4)/MCM41 revealed the increase in the concentration of Cr⁶⁺ species which interacted with the framework of siliceous support. On the other hand, H₂-TPR profiles of Cr(4)-Co(4)/MCM41 showed wide reduction peaks centered at 400 °C which is ascribed to reduction of Cr⁶⁺ to Cr³⁺ species and Co₃O₄ to metallic Co. At the same time, Cr(4)-Mo(4)/MCM41 and Cr(4)-V(4)/MCM41 exhibited higher temperature reduction peaks, indicating these two catalysts require higher activation temperatures. The synergy between the Cr with Zn or Nb metals reduced the concentration of Cr⁶⁺ species which is reflected in their catalytic performance. Cr(4)-Ce(4)/MCM41 recorded the highest catalytic activity toward ethylene production where the ethane conversion and ethylene yield were 37.9% and 35.1%, respectively.

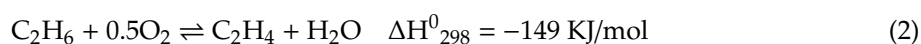
Keywords: bimetallic oxide; Cr-based catalyst; mesoporous silica; ethane oxidative dehydrogenation; CO₂

1. Introduction

Ethylene, a crucial material in the petrochemical industry, is used in the production of versatile intermediate and final products. Commercially, ethylene is produced by catalytic cracking and steam cracking of hydrocarbon feedstocks like ethane and naphtha [1,2].



The cracking processes, Equation (1), have several drawbacks, including high energy requirements because of its endothermicity, severe coke formation, thermodynamic limitation, and inefficient control of ethylene selectivity [3–5]. Oxidative dehydrogenation of ethane by oxygen, Equation (2), has been introduced as a good alternative to the thermal cracking process because coke formation is minimized because of the presence of oxygen [6,7].



However, over-oxidation of ethane and ethylene to carbon oxides and the probable formation of hot spots are the major issues of this process [8,9]. On the other hand, utilization of CO₂ as a mild oxidant in ethane dehydrogenation, Equation (3), has received enormous interest in recent years. It has been established that using CO₂ improves the yield and selectivity of ethylene as well as maintains the catalytic activity by reducing coke formation [10,11].



Various catalytic systems containing active species, such as: Cr [1,8,12–28], Ga [29–34], Ce [35,36], Zn [34], Co [37–40], La [41,42], Fe [43], V [44,45], Ni [40,42,46], Mo [40,47], In [48], and Mn [43,49] have been investigated for oxidative dehydrogenation (ODH) of light alkanes with CO₂. Among the investigated catalytic systems, chromia-based catalyst emerged as the most promising catalytic system for this reaction [8,15,16,21,28]. So far, different metal oxide supports for chromia like Cr₂O₃/Al₂O₃, Cr₂O₃/SiO₂, Cr₂O₃/ZrO₂, and Cr₂O₃/TiO₂ [8], Cr₂O₃/ZSM-5 [11], modified Cr₂O₃/ZrO₂ [16], Cr₂O₃/CeO₂, Cr₂O₃/Ce_xZr_(1-x)O₂, and Cr/SBA-15/Al₂O₃/FeCrAl monoliths [23]. Even though, silica-supported chromia is well-known to be the most active catalyst for the ODH of ethane with CO₂, however, their catalytic activity is still insufficient for commercial application; therefore more work is still needed to improve ethane conversions and ethylene yield.

Bimetallic and multi-metallic catalysts have gained much attention in recent years [50–52]. Proper synthesis and characterization of uniformly dispersed supported bi-metallics could provide a synergistic effect that usually enhances the catalytic activity and/or selectivity toward one of the products [52–54]. Myint et al. [40] compared the catalytic activity of CoPt/CeO₂, CoMo/CeO₂, NiMo/CeO₂, and FeNi/CeO₂ bimetallic catalysts for the reaction of ethane with CO₂. They found that the catalytic stability was enhanced in all bimetallic catalysts. In terms of selectivity, the reaction favored the reforming pathway over CoPt/CeO₂, CoMo/CeO₂, and NiMo/CeO₂ catalysts while FeNi/CeO₂ showed promising selectivity to ODH pathway [40]. Moreover, Jibril et al. [55] tested MCM41-supported NiMo and CoMo bimetallic catalysts for oxidative dehydrogenation of propane to propylene. Taghavinezhad et al. [56] synthesized Mg-, Al-, Zr-modified VO_x/MCM-41 catalyst to assess the impact of modification of vanadium-based MCM41 materials on ODH of ethane with CO₂. The results revealed that addition of various metal oxides affected the catalytic activity of the modified catalysts by altering their structural properties, such as crystallinity, particle sizes, and dispersity of the modified vanadium species along with their acid/base properties. On the other hand, Le et al. [57], have employed cerium oxide to promote nano-size Na-ZSM-5 after chromium oxide loading; the developed catalyst was tested for the ODH of ethane by using CO₂. It was found that the introduction of Ce species clearly improves the dispersity of Cr species on the surface of Na-ZSM-5 catalysts which enhanced the catalytic activity and stability of the prepared catalyst, and reduced the amount of carbon formed on the catalyst surface at the same time. Shi et al. [58] showed that the introduction of Ce species to Cr/SBA-15 catalysts has remarkable impact on changing the redox properties which in turn has improved the catalytic activity of chromium oxide species.

In the present work, the synergetic impact of a secondary metal oxide (M) of Cr-M/MCM41 catalyst system for ethane oxidative dehydrogenation using carbon dioxide was investigated. The effect of the secondary metal oxide (Co, Ce, Zn, Nb, V, and Mo) on the textural, physical, and chemical properties of Cr-M/MCM41 catalysts were evaluated. The main aim of this study is to assess the effect of the secondary metal on the activity behavior of the catalysts for the ODH of ethane.

2. Experimental

2.1. Materials

Tetraethyl orthosilicate [$\text{Si}(\text{OC}_2\text{H}_5)_4$, TEOS, $\geq 98\%$] (silica precursor) and cetyltrimethylammonium chloride [CTAC, 25 wt.% aqueous solution] (cationic surfactant) were obtained from Sigma-Aldrich, (Steinheim, Germany). Chromium nitrate nonahydrate [$\text{Cr}(\text{NO}_3)_3 \cdot 9\text{H}_2\text{O}$], niobium oxalate hydrate [$\text{C}_{10}\text{H}_5\text{NbO}_{20} \cdot x\text{H}_2\text{O}$], and ammonium vanadium oxide [NH_4VO_3] were obtained from Alfa Aesar (Karlsruhe, Germany) while cerium(III) nitrate hexahydrate [$\text{Ce}(\text{NO}_3)_3 \cdot 6\text{H}_2\text{O}$], cobalt nitrate hexahydrate [$\text{Co}(\text{NO}_3)_2 \cdot 6\text{H}_2\text{O}$], zinc nitrate hydrate [$\text{Zn}(\text{NO}_3)_2 \cdot x\text{H}_2\text{O}$], and ammonium molybdate tetrahydrate [$(\text{NH}_4)_6\text{Mo}_7\text{O}_{24} \cdot 4\text{H}_2\text{O}$] were ordered from Sigma-Aldrich (Steinheim, Germany). These chemicals were used as precursors of metal oxides in this study. All other reagents were also obtained from Sigma-Aldrich and used as-received without further purification. Moreover, ammonium hydroxide solution [NH_4OH , 28.0–30.0%] (the precipitating agent) was supplied from Sigma-Aldrich.

2.2. Catalyst Preparation

According to precipitation behavior of the metal oxide precursor in the basic media, the secondary metal salts were loaded into Cr-MCM41, either by one-pot co-precipitation approach or through impregnation method [27]. Cr(4)-M(4)/MCM41 (M = Ce, Co, and Zn) catalysts were prepared by one pot-synthesis while Cr(4)-M(4)/MCM41 (M = Mo, V and Nb) that do not precipitate in basic medium, Cr-MCM41 was formed first by one-pot synthesis and then the secondary metal salts were impregnated on Cr(4)/MCM41 samples. In a typical synthesis, 4.40 ml of CTAC, 52.5 ml of distilled water, and 4 ml of ammonium hydroxide were added to prepare a homogeneous solution, which was stirred (400 rpm) for 10 min. After that, a solution of exact amount of Cr and M (M = Ce, Co, and Zn) precursors was added with stirring for 60 min. Then under a vigorous stirring, 4.94 ml of TEOS was added dropwise for further 60 min. After that the resultant precipitant was filtered, washed, and dried at 80 °C overnight. The dried sample was then calcined in air by heating it from ambient temperature to 650 °C over a 5-h period and keeping it at 650 °C for another 12 h. On the other hand, preparation of Cr(4)-M(4)/MCM41 (M = Mo, V and Nb) catalysts started by synthesizing Cr(4)/MCM41 sample using the one-pot synthesis procedure and the secondary metal salt was impregnated on Cr(4)/MCM41 samples. The catalysts were denoted as Cr(4)-M(4)/MCM41, where 4 stands for nominal Cr and M total contents given in wt.% of Cr and M respectively.

2.3. Catalyst Characterization

X-ray diffraction spectra were obtained for all prepared bimetallic oxide catalysts by using (PANalytical X'Pert PRO MPD) (PANalytical, Netherlands). The isotherms of nitrogen sorption were determined after the samples were evacuated at 200 °C for 3 h to remove adsorbed gases and vapors. The pore size distribution of Cr(4)-M(4)/MCM41 catalysts were analyzed from the desorption profiles of the isotherms by employing the Barrett-Joyner-Halanda (BJH) method. Diffuse reflectance UV–vis spectrum was obtained for the 230–700 nm range by Shimadzu 2550 spectrophotometer (Shimadzu, Kyoto, Japan). The reducibility of the prepared bimetallic oxide catalysts was measured by hydrogen temperature programmed reduction (H₂-TPR) by Micromeritics Auto Chem II apparatus (Micromeritics, Norcross, GA, USA) To reveal the surface morphology of the prepared samples, Energy-dispersive X-ray elemental-mapping were performed using JEOL JEM-7500F scanning electron microscope (SEM)

(JEOL, Tokyo, JAPAN) JEOL JEM-2100F transmission electron microscope (TEM) (JEOL, Tokyo, JAPAN) operated at 200 kV was used to determine the internal structure of the samples.

2.4. Catalyst Evaluation

Figure 1 depicts the experimental setup used for the ODH of C_2H_6 with CO_2 over the bimetallic oxide catalysts. The experiments were carried out by using 300 mg of the prepared catalysts sandwiched between two layers of glass wool. The catalyst samples were first pretreated in situ at 600 °C in air flowing at 18 mL/min for 0.5 h. Ethane dehydrogenation with carbon dioxide was performed at atmospheric pressure and reaction temperature range 600–700 °C. The reactants mixture was fed into the reactor with a total flow rate of 75 ml/min. The feed was composed of 7.5 C_2H_6 , 37.5 CO_2 , and 30 ml/min N_2 respectively. The reaction products as well as unconverted substances were analyzed after 20 min from the beginning of the ODH reaction. The analysis of the various components was conducted by an online gas chromatograph coupled with FID and TCD detectors (Agilent 6890N, Agilent, Santa Clara, CA, USA) and using molecular sieve 5Å hayesepQ and gas pro(Sigma-Aldrich/supelco, Taufkirchen, Germany) as GC columns. Before the analysis the formed water was trapped from the analysis samples. Also, blank tests were performed to confirm that the homogenous reaction is negligible at the experimental conditions.

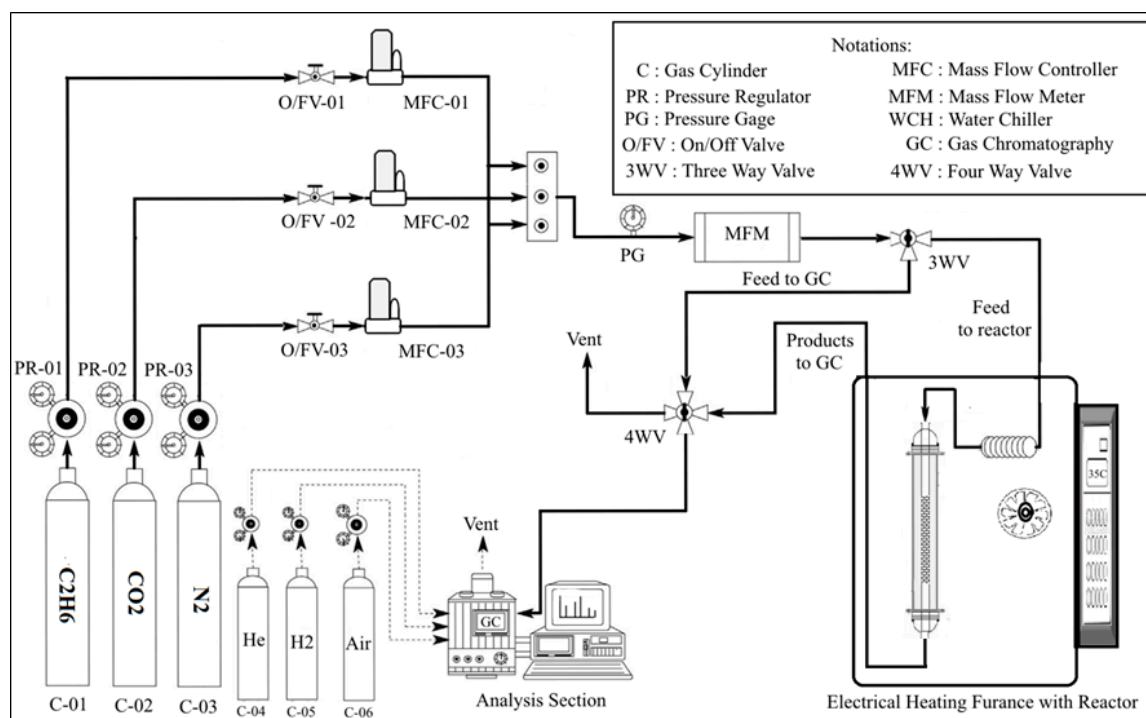


Figure 1. Experimental setup for the oxidative dehydrogenation of ethane with CO_2 .

The conversion of ethane, yield of ethylene, and selectivity of products were calculated based on Equations (4)–(6);

$$\text{Ethane Conversion (\%)} = \frac{F_{C_2H_6_{in}} - F_{C_2H_6_{out}}}{F_{C_2H_6_{in}}} \times 100 \quad (4)$$

$$\text{Ethylene Yield (\%)} = \frac{F_{C_2H_4}}{F_{C_2H_6_{in}}} \times 100 \quad (5)$$

$$\text{Ethylene Selectivity (\%)} = \frac{F_{C_2H_4}}{F_{C_2H_4} + F_{CH_4}} \times 100 \quad (6)$$

where F_j = No. of moles of component j.

3. Results and Discussion

3.1. Catalysts Characterization

XRD analysis was performed to study the crystallographic properties of the bimetallic oxide catalysts, and the diffraction patterns are shown in Figure 2. The diffraction peaks observed at $2\theta = 24.5, 33.6, 36.2, 41.5, 50.2, 54.9, 63.4,$ and 65.18° corresponding to (012), (104), (110), (113), (023), (116), (212), and (300) planes confirmed the presence of the rhombohedral Cr_2O_3 crystals (JCPDS 00-006-0504) in each catalyst [17]. The intensity of Cr_2O_3 peaks depends on the secondary element of the bimetallic system. While it is low for Cr-Co/MCM41 and Cr-Zn/MCM41, it is relatively high for Cr-Mo/MCM41. The low intensity of the peaks signifies the formation of small particle size of Cr species and also their fine dispersion on the surface of the catalyst. In contrast, no change was observed in Cr_2O_3 peaks intensity of Cr-Ce/MCM41, Cr-Nb/MCM41, and Cr-V/MCM41 catalysts. In addition to Cr_2O_3 , other peaks were observed at different values of 2θ which confirm the presence of the secondary metal oxides MO_x ($M = \text{Co}, \text{Ce}, \text{Zn}, \text{Nb}, \text{V}, \text{Mo}$) in the catalysts. The Cr-Co/MCM41 catalyst shows more diffraction peaks at $2\theta = 30.5, 36.1, 44.4,$ and 58.4° corresponding to the (220), (311), (400), and (511) planes which can be indexed to a cubic structure of Co_3O_4 phase (JCPDS NO. 76-1802).

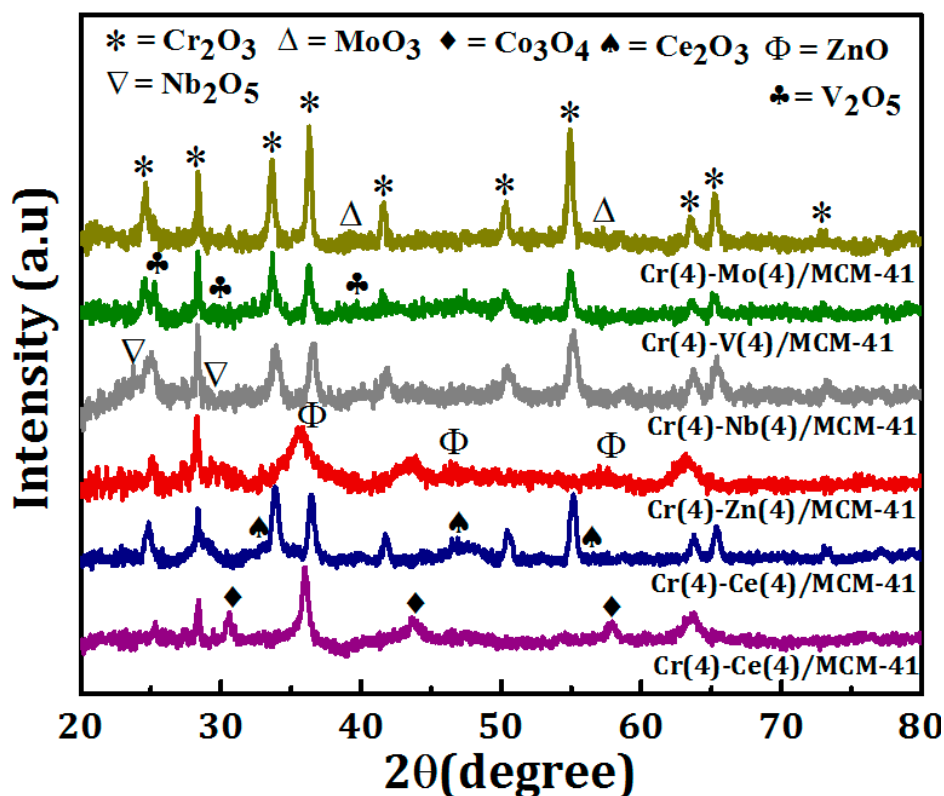


Figure 2. X-ray diffraction (XRD) patterns of Cr(4)-M(4)/MCM-41 bimetallic oxide catalysts.

In the case of Cr-Ce/MCM-41, the peaks observed at $2\theta = 28.4, 33.1, 47.5^\circ$, corresponding to the (111), (200), (220), and (311) planes, were indexed to the presence of cubic, fluorite structure of CeO_2 [59]. The diffraction peaks observed at $2\theta = 29, 36.8, 50.4,$ and 55.2° for Cr-Nb/MCM41, corresponding to the (180), (181), (380), and (212) planes, and related to the presence Nb_2O_5 in the catalyst. In the case of Cr-V/MCM41 the diffraction peaks observed at $2\theta = 25.1, 29.8, 39.4,$ and 50.30 were indexed to the presence of V_2O_5 . The XRD pattern of Cr-Mo/MCM41 showed that in addition to Cr_2O_3 peaks there are more diffraction peaks at $2\theta = 29, 36.8, 50.4,$ and 55.2° which confirm the presence of MoO_2 and MoO_3 on the catalyst surface [60].

The isotherms of N₂ sorption and the distribution of the pore sizes of the bimetallic oxide Cr(4)-M(4)/MCM41 catalysts are presented in Figure 3A,B. The textural properties of these catalysts are displayed in Table 1.

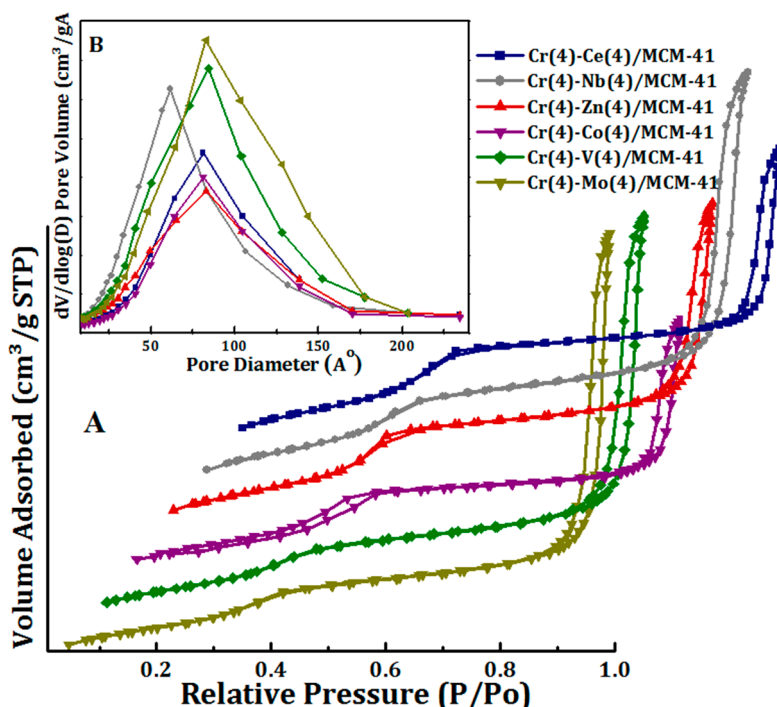


Figure 3. (A) N₂ sorption isotherms and (B) pore size distribution of Cr(4)-M(4)/MCM41 bimetallic oxide catalysts.

Table 1. Textural properties of Cr(4)-M(4)/MCM41 bimetallic catalyst.

Catalyst	BET (m ² /g)	Pore Volume (cm ³ /g)	Pore Size (nm)
Cr-Zn/MCM41	865	1.71	7.29
Cr-Co/MCM41	878	1.42	5.72
Cr-C/MCM41	886	1.62	6.73
Cr-V/MCM41	721	2.08	10.86
Cr-Nb/MCM41	880	2.16	9.41
Cr-Mo/MCM41	701	2.14	11.83

The Cr(4)-M(4)/MCM-41 catalysts exhibit type IV isotherm with H1 hysteresis loop which is a standard profile for mesoporous materials according to the IUPAC classification. This confirms that the MCM-41 mesoporous structure was stable and not altered by the addition of the secondary metal oxides (Figure 3). It can be seen that, the hysteresis loop of Cr-Co/MCM41 that appears at relative pressure P/P₀ = 0.2–0.55 clearly proves that its porous feature possess uniform cylindrical pore geometry. On the other hand, the hysteresis loops of Cr(4)-M(4)/MCM41 (Me=Co, Ce, Zn, Nb, V, and Mo) appeared at relatively higher pressures which obviously demonstrated the formation of mesoporous with larger pore diameter [61]. Figure 3 shows the pore size distribution of the synthesized bimetallic oxide catalysts. All Cr(4)-M(4)/MCM41 catalysts showed wide pore size distribution centered at 6 nm for Cr-Nb/MCM41 sample, and at 10 nm for Cr-Mo/MCM41 and Cr-V/MCM41. On the other hand, pore size was 8 nm for Cr-Ce/MCM41, Cr-Co/MCM41, and Cr-Zn/MCM41. Moreover, the synthesized bimetallic oxide catalysts revealed high BET surface area (701–886 m²/g) and it was in the order of Ce(4) > Nb(4) > Co(4) > Zn(4) > V(4) > Mo(4).

The reducibility of supported MCM41 bimetallic oxide catalysts was investigated using H₂-TPR and the comparison between these catalysts is shown in Figure 4A,B. H₂-TPR profiles of bimetallic

oxide catalysts showed that the reduction peaks of each bimetallic system differ totally from those observed in literature for Cr-monometallic ones [62], suggesting a synergistic interaction between the two elements had taken place. The H₂-TPR profile of Cr-Ce/MCM41 displayed a slight shift of both reduction peaks to higher temperatures with decreasing intensity of the first peak and increasing the second one compared to those of monometallic Cr catalyst [62]. However, these results indicated the decrement of the concentration of free Cr⁶⁺ species which are dispersed on the surface of crystalline α -Cr₂O₃ along with the increment of concentration of Cr⁶⁺ species which interacted with the MCM-41 structure. Moreover, new broad peak centered on 750 °C arose which are assigned to reduction of ceria oxide that interacted with MCM41 matrix. On the other hand, H₂-TPR profile of Cr-Co/MCM41 had two wide reduction peaks centered at 400 and 650 °C respectively. The first peak is attributed to the reduction of Cr⁶⁺ to Cr³⁺ species and Co₃O₄ to metallic Co, whereas the second broad one illustrates the reduction of Co²⁺ species that is highly dispersed and strongly interacted with the surface of MCM41 [62].

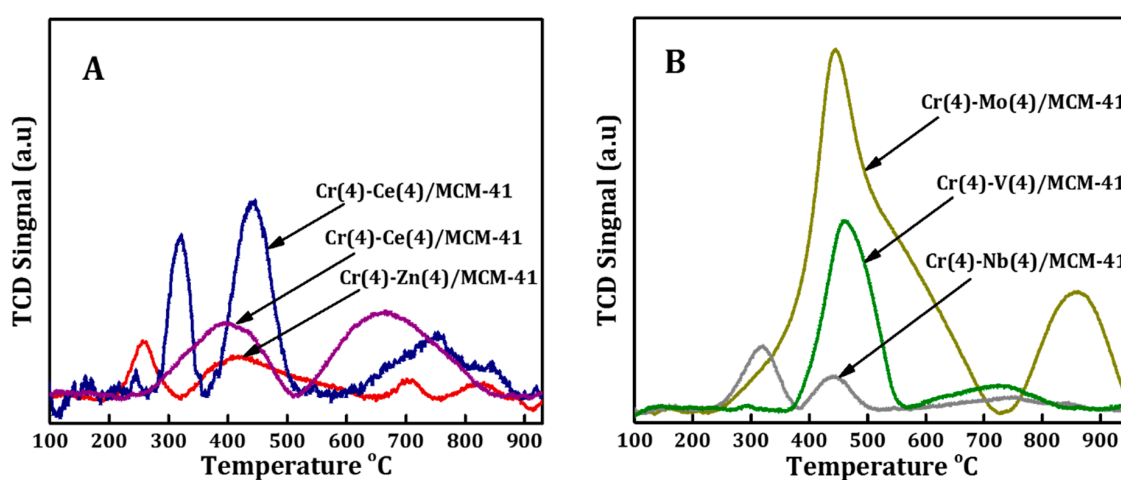


Figure 4. Hydrogen temperature programmed reduction (H₂-TPR) profiles spectrum of Cr(4)-M(4)/MCM41 bimetallic oxide catalysts prepared by (A) one-pot synthesis approach and (B) prepared by impregnation method.

In the case of Cr-Zn/MCM41, the intensity of the two peaks decreased compared to those of monometallic-Cr catalyst [62] while the higher temperature peak observed at 700 °C suggested that most of the chromium was formed in bulk chromium oxide.

At the same time, H₂-TPR profiles of the catalysts prepared with the impregnation method is shown in Figure 4B. In the case of Cr-Mo/MCM41, the peak at low temperature (250 °C) disappeared [62]; the second reduction of monometallic Cr overlapped with the reduced Mo and a new peak centered at 850 °C was detected. The second peak shape indicates that there are multiple peaks overlapping at temperatures above 500 °C. These multiple peaks reflected the complex interaction of Mo species with different oxidation states on the MCM41 matrix. Arnoldy and his colleagues [63] reported that the low temperature peak is formed due to the reduction of octahedrally Mo⁶⁺ multilayer while the peak at higher temperature (850 °C) is related to the reduction of tetrahedrally and octahedrally Mo⁶⁺ monolayer species. However, the pronounced peak at around 460 °C has been associated with the reduction of Cr⁶⁺ to Cr³⁺ species and octahedral Mo species.

H₂-TPR profile of Cr-V/MCM-41 bimetallic catalyst showed the increment of the second peak temperature (460 °C) along with a broader peak centered around 720 °C. The main peak is related to the reduction of the dispersed Cr⁶⁺ species as well as the tetrahedral vanadium species, while the broader one could be related to the reduction of polymeric V⁵⁺ species [64]. The Cr-Nb/MCM-41 bimetallic oxide catalyst showed a slight shift of both peaks toward higher reduction temperature with a large drop in the peaks intensity, indicating the domination of unreducible chromium. H₂-TPR profiles of

Cr-Ce/MCM41 and Cr-Co/MCM41 exhibited the highest intensity of Cr^{6+} peaks which suggested the formation of high concentration of interacted Cr^{6+} with silica matrix that acts as active sites for alkane dehydrogenation with CO_2 [27,62].

The presence of different oxidation states of Cr (Cr^{6+} and Cr^{3+}) on the surface of bimetallic catalysts was investigated with UV-Vis diffuse reflectance spectroscopy and the spectra are shown in Figure 5. All spectra showed two main absorption bands at 270 and 370 nm. These two bands originate from $\text{O}^{2-} \rightarrow \text{Cr}^{6+}$ charge transfer transition of chromate species in tetrahedral coordination [65–67]. A shoulder band observed at around 415 nm, in Cr(4)-M(4)/MCM41 (M = Ce, Co, V, Nb, and Mo) samples, is assigned to dichromates or poly-chromates on the catalysts surface [68,69]. This shoulder had disappeared in case of Cr-Zn/MCM41 and overlapped with the band at 470 nm for Cr-Zn/MCM41. On the other hand, the absorption bands at 470 and 600 nm are referred to d-d transitions of Cr^{3+} species in the octahedral symmetry [12,68,70–73]. It can be observed that the Cr^{3+} bands disappeared in the Cr-Zn/MCM41 and Cr-Nb/MCM41 samples. As it has already been established that Cr^{3+} and Cr^{6+} coexist on the surface of Cr/silica catalysts and the highly dispersed Cr^{6+} species is believed to constitute the active sites in ODH of alkanes [18,71,74–76].

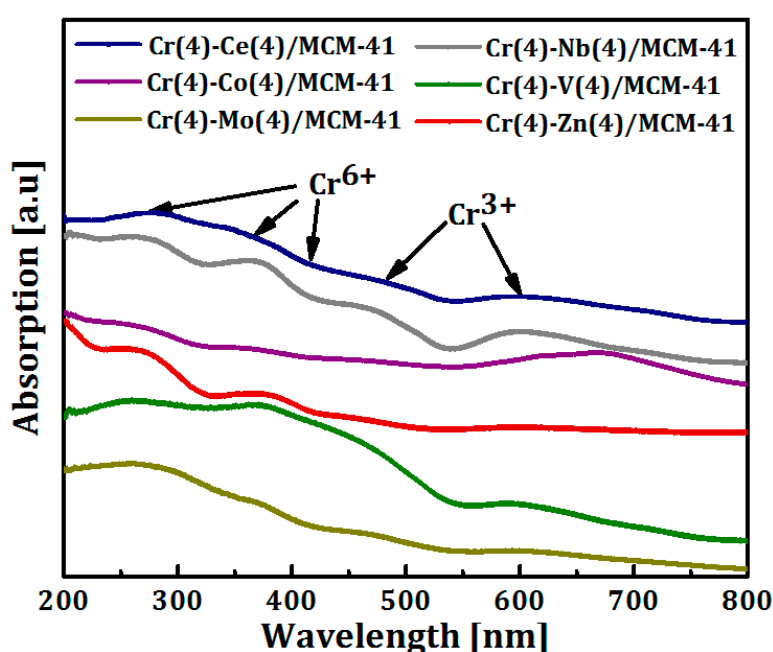


Figure 5. UV-Vis-DR spectra of Cr(4)-M(4)/MCM41 bimetallic oxide catalysts.

SEM observation as well as EDX elemental mapping were conducted for two selected samples, Cr(4)-Ce(4)/MCM41 and Cr(4)-Co(4)/MCM41 to estimate the state of dispersion in both catalysts and the results are presented in the Figure 6. SEM images for Cr-Ce (Figure 6a) and Cr-Co (Figure 6b) showed the irregular structure of the formed nanoparticles agglomerates; no pronounced effect was observed when changing the secondary metal oxide from Ce to Co. Elemental mapping for Cr (blue) showed homogenous distribution over the surface of mesoporous silica nanoparticles (red color). However, Cr-Ce sample showed a relatively bigger size of the formed CrO_x species than Cr-Co sample. On the other hand, Ce (green) and Co (cyan) mapping suggested that both oxides have good and homogeneous distribution. The good distribution of CrO_x , CeO_2 and Co_3O_4 suggested that these oxides diffused into the mesochannels of mesoporous silica along with their formation onto the outer surface as well.

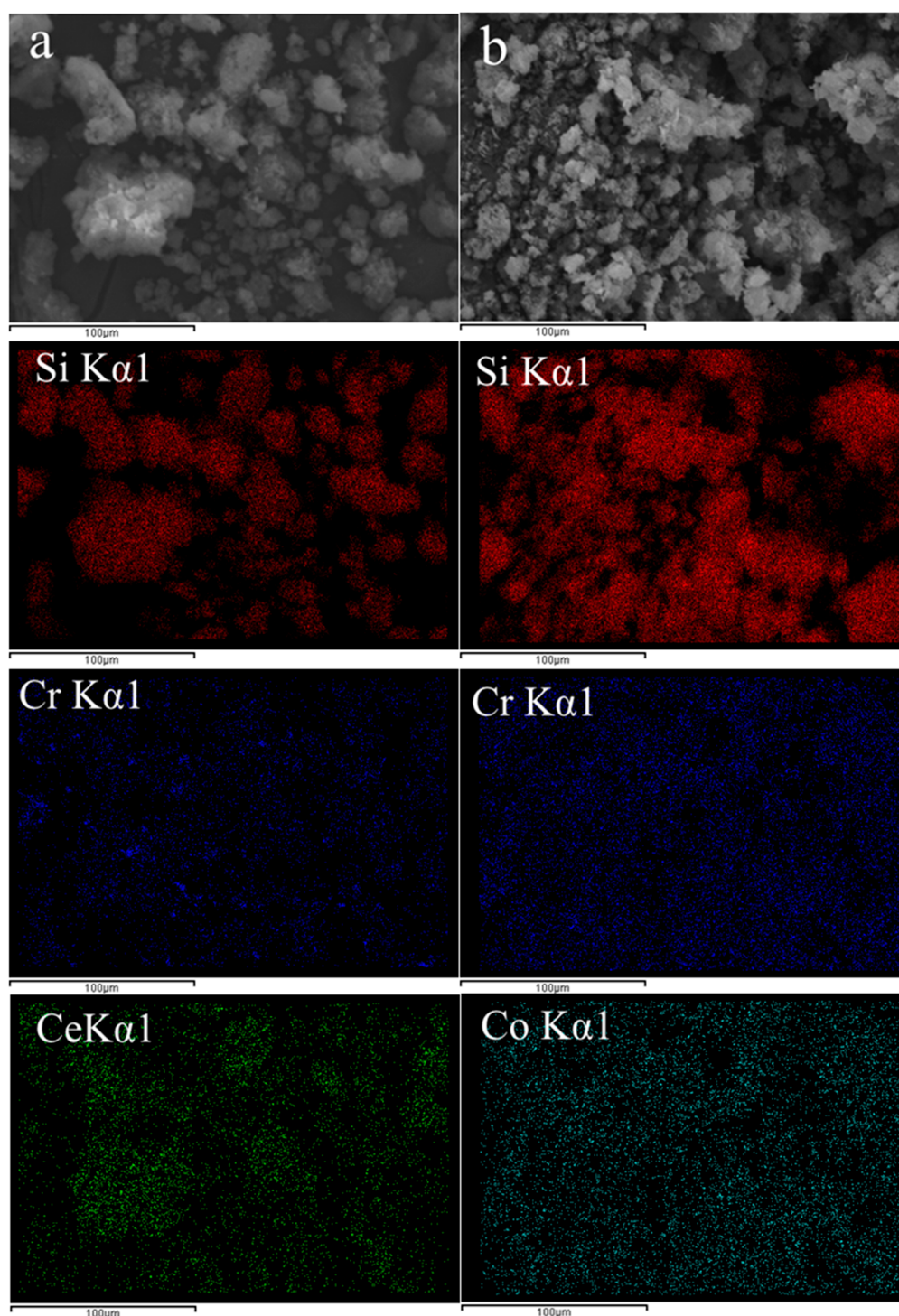


Figure 6. Scanning electron microscopy (SEM) images and EDX elemental mapping (silicon (red), chromium (blue), cerium (green), cobalt (cyan)) of (a) Cr-Ce/MCM41 and (b) Cr-Co/MCM41.

TEM observations have been carried out for two samples, Cr-Ce/MCM41 and Cr-Co/MCM41, to get more insight of the internal structure and the images are displayed in the Figure 7. Cr-Ce/MCM41 sample, Figure 7Aa, showed the formation of CrOx and CeO₂ species into the surface of mesoporous silica. The CrOx nanoparticles showed rod-like morphology while CeO₂ had irregular shape. The sizes of CrOx and CeO₂ nanoparticles were estimated to be 130 and 53 nm, respectively. On the other hand, TEM image of Cr-Co/MCM41 sample, Figure 7Aa', revealed that Co₃O₄ nanoparticles were

round-shaped with fine size of 15–25 nm while CrO_x species nanoparticles possessed rhombohedral shape with bigger sizes of 130 nm.

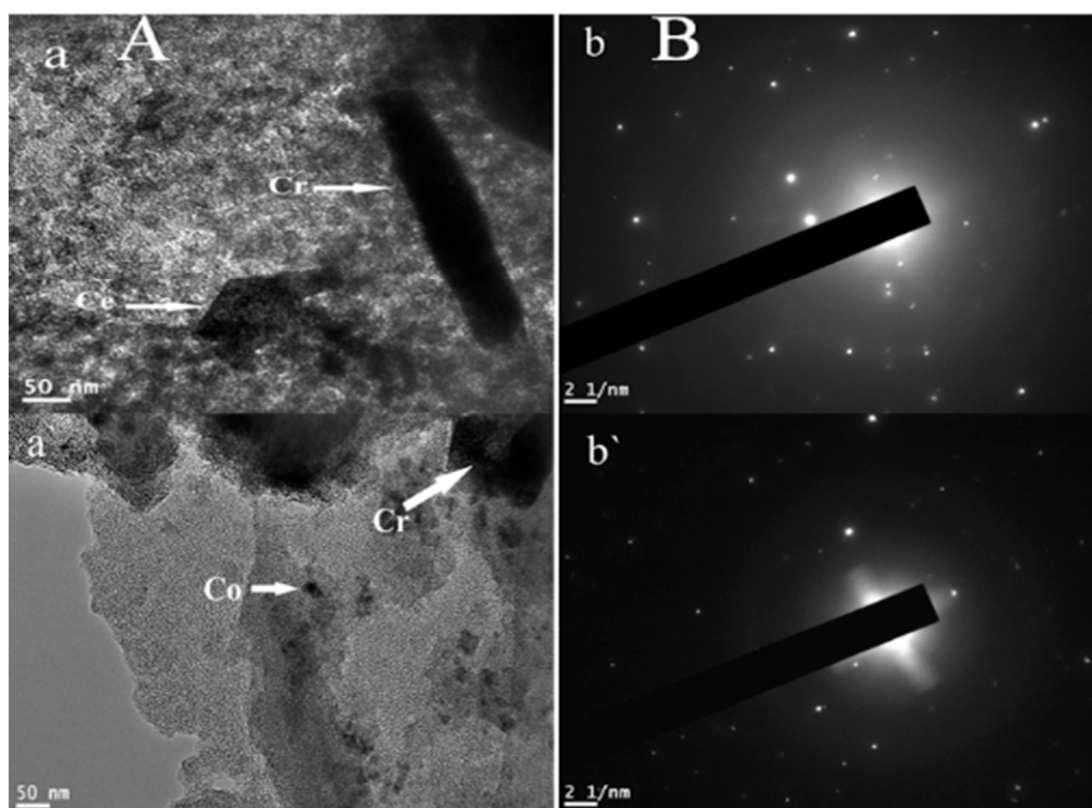


Figure 7. (A) Transmission electron microscopy (TEM) images of (a) Cr-Ce/MCM41 and (a') Cr-Co/MCM41 and (B) selected area electron diffraction (SAED) images of (b) Cr-Ce/MCM41 and (b') Cr-Co/MCM41.

The TEM results complement SEM elemental mapping results that showed more homogenous distribution of Cr, Ce, and Co on the surface of mesoporous silica. The results agree with the previous findings that the catalysts will fill first the mesochannels of mesoporous silica and thereafter they begin to form onto outer surface [62]. This mechanism provided the rod-like Cr and irregular Ce nanoparticles in case of Cr-Ce sample and rhombohedral Cr and round Ce nanoparticles as in case of Cr-Co sample.

The selected area electron diffraction (SAED) have been conducted for Cr(4)-Ce(4)/MCM41 and Cr(4)-Co(4)/MCM41 and are displayed in Figure 7Bb and 7Bb', respectively. It is clear that Cr-Ce/MCM41 in Figure 7Bb possess poly-crystallinity with spot pattern because of the co-existence of poly-crystalline CrO_x and CeO₂ nanoparticles. On the other hand, Cr-Co/MCM41 in Figure 7Bb' reveal that the samples has rhombohedral spot pattern that can be attributed to the formation of large size rhombohedral mono-crystalline CrO_x. Because of the small sizes of Co₃O₄ nanoparticles, they did not appear into SAED pattern.

3.2. Catalytic Activity of Cr(4)-M(4)/MCM41 Catalysts

The catalytic performance of Cr(4)-M(4)/MCM41 bimetallic oxide catalysts were investigated in ODH of C₂H₆ with CO₂ at different reaction temperatures and the results are presented in Figure 8. Generally, it can be observed that for all bimetal oxide catalysts, both the C₂H₆ conversion and the C₂H₄ yield increased with rising of reaction temperature because of the endothermicity of the reaction. On the other hand, the ethylene selectivity dropped slightly with temperature, indicating

that hydrocracking of ethane and ethylene are favorable at high reaction temperatures. Also it can be noted that Cr-Ce/MCM41 and Cr-Co/MCM41 catalysts have the highest catalytic performance among the prepared samples. 37.9% C₂H₆ conversion and 35.1% C₂H₄ yield were obtained for the Cr-Ce/MCM41 catalyst and 36.1% of ethane conversion with 33.7% ethylene yield was recorded for the Cr-Co/MCM41 catalyst.

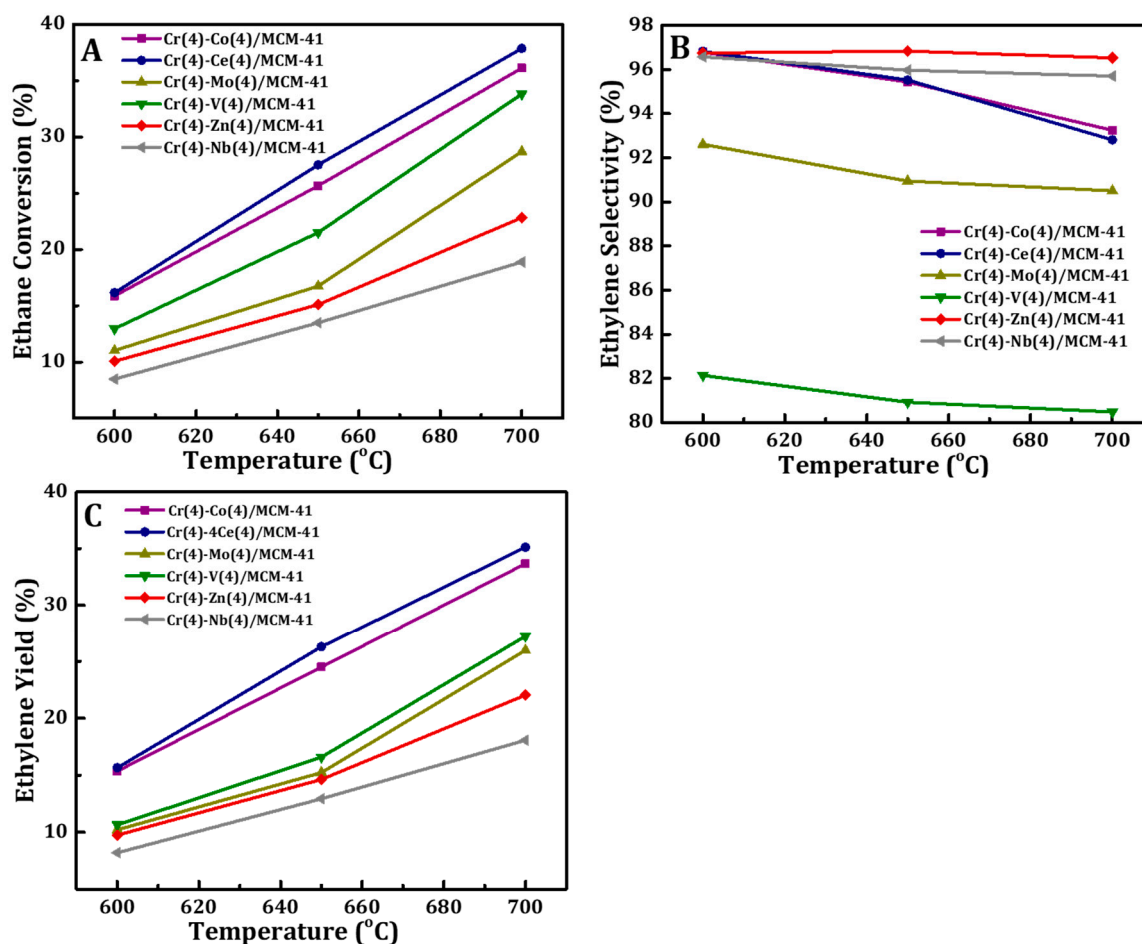


Figure 8. Effect of reaction temperature on (A) ethane conversions, (B) ethylene selectivity, and (C) yield of Cr(4)-M(4)/MCM41 bimetallic oxide catalyst.

For the Cr-based catalytic system it is well-known that Cr⁶⁺ is the key factor to higher catalytic activity in the oxidative dehydrogenation of ethane [71,77]. In this study, the characterization results show that the addition of Ce or Co species increased the reducibility of Cr⁶⁺ and the ratio of interacted Cr⁶⁺ with silica matrix. In addition, the higher catalytic activity of Cr-Ce/MCM41 and Cr-Co/MCM41 catalysts may also be caused by the presence of Ce and Co species respectively, which enhanced their performance because of the redox property of CeO₂ and Co₃O₄ as well as synergy. Valenzuela et al. [35] and Sharma et al. [78] reported that the redox Ce⁴⁺/Ce³⁺ of CeO₂ can activate CO₂ to produce active oxygen species for the ODH of ethane reaction. On the other hand, Cr-V/MCM41 showed low catalytic activity in the oxidative dehydrogenation of ethane with CO₂ where lower values of ethane conversion and ethylene yield were observed over this bimetallic oxide catalyst. Moreover, the selectivity to ethylene showed a decay trend over Cr-V/MCM41, suggesting further oxidation of the produced ethylene.

It was found that the reaction temperature has a strong influence on the catalytic performance of vanadium oxide-based catalytic system and it is mainly related to the reducibility of the active sites (V atoms) [64,79–81]. However, Cr-V/MCM41 catalyst may need much higher temperature to be

active for ODH of ethane reaction. This assumption is consistent with H₂-TPR measurement where the reduction temperatures of this catalyst have shifted to higher temperature. The same trend can be concluded for the other three catalysts, Cr(4)-M(4)/MCM41 (M = Zn, Nb, Mo), which showed much lower catalytic activities compared to Cr-Ce/MCM41 and Cr-Co/MCM41 catalysts. Finally, the synergy between the Cr and Zn or Nb oxides led to a drop in the catalytic activity toward ethylene production. This drop is related to the reduction of Cr⁶⁺ on the surface of these two catalysts. The catalytic activity of synthesized bimetallic oxide catalysts can be arranged in the following sequence: Ce(4) > Co(4) > V(4) > Zn(4) > Nb(4) > Mo(4).

The stability of Cr(4)-M(4)/MCM41 bimetallic oxide catalysts was investigated by running continuously the ODH of ethane with CO₂ reaction for more than 8 h. The results are presented in Figure 9. It can be seen that, the catalytic activity of all synthesized bimetallic oxide catalysts, in terms of C₂H₆ conversion and C₂H₄ yield, decreased slowly with increasing reaction period. On the other hand, the C₂H₄ selectivity almost remains stable above 91% even after 8 h. Drop of highly reducible Cr species in addition to coke formation are the expected reasons for such a decline in catalytic performance. However, Cr-Ce/MCM41 and Cr-Co/MCM41 catalysts still showed acceptable catalytic properties after 8 hours on stream reaction. The reasonable stability of these catalysts can be referred to the high reducible Cr species on the surface of these samples.

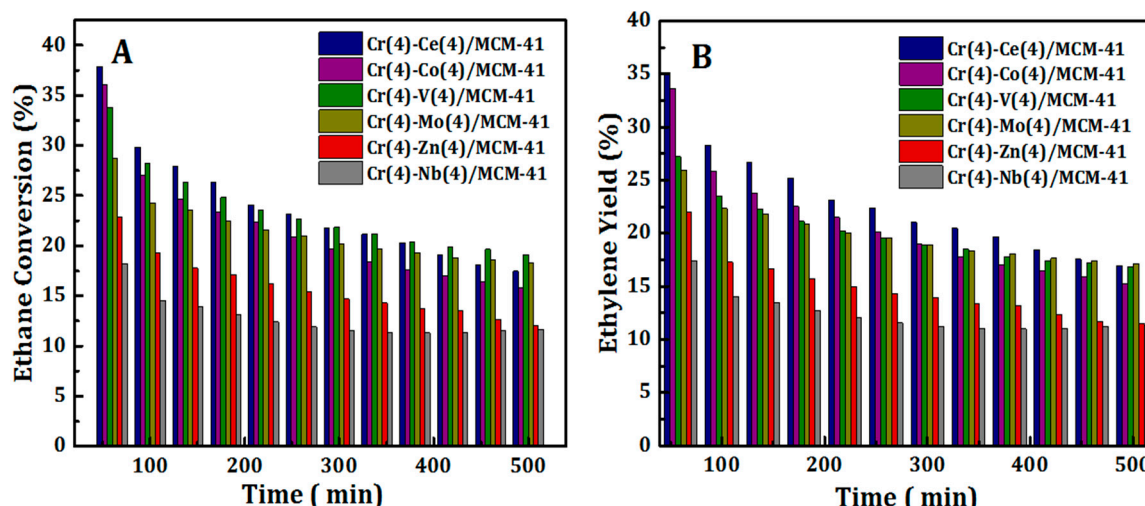


Figure 9. Variation of C₂H₆ conversion (A) and C₂H₄ yield (B) with time on stream over Cr(4)-M(4)/MCM41 bimetallic oxide catalysts.

4. Conclusions

MCM41 supported bimetallic oxide catalysts containing chromium oxide along with a secondary metal oxide (Ce, Co, Zn, V, Mo, or Nb) were prepared. The prepared catalysts have been characterized and evaluated for ODH of ethane by using CO₂ as an oxidant. Cr-Ce/MCM41 and Cr-Co/MCM41 exhibited catalytic activity which can be correlated to the high population of redox sites on their surfaces as indicated by H₂-TPR along with good dispersion of Cr and Ce and Co oxide species and high textural properties. On the other hand, Cr-V/MCM41 and Cr-Mo/MCM41 showed a significant drop in the activity and the selectivity to ethylene. While Cr-Zn/MCM41 and Cr-Nb/MCM41 exhibited the highest selectivity to ethylene, their activity was much lower than Cr-Ce/MCM41 and Cr-Co/MCM41 catalysts. The results suggested that Cr-Ce/MCM-41 and Cr-Co/MCM-41 possessed promising potentials as catalysts for converting ethane to ethylene; however further studies are still required to optimize their loading content to enhance the catalytic performances.

Author Contributions: Conceptualization, writing-review editing: A.E.A. and S.M.A.-Z. Investigation, writing-original draft, writing-review editing: A.S.A.-A., A.M.E.-T., and A.E.A. Methodology and formal

analysis: A.S.A.-A., M.A., A.K., M.A.S., A.S.A.-A. and A.M.E.-T. All authors have read and agreed to the published version of the manuscript.

Funding: This work was funded by Researchers Supporting Project number (RSP-2019/90), King Saud University, Riyadh, Saudi Arabia.

Conflicts of Interest: The authors declare no conflict of interest.

References

1. Ramesh, Y.; Thirumala Bai, P.; Hari Babu, B.; Lingaiah, N.; Rama Rao, K.S.; Prasad, P.S.S. Oxidative dehydrogenation of ethane to ethylene on $\text{Cr}_2\text{O}_3/\text{Al}_2\text{O}_3\text{-ZrO}_2$ catalysts: The influence of oxidizing agent on ethylene selectivity. *Appl. Petrochem. Res.* **2014**, *4*, 247–252. [[CrossRef](#)]
2. Leena, K. International survey of ethylene from steam crackers. *Oil Gas. J.* **2012**, *2*, 85.
3. Dharia, D.; Letsch, W.; Kim, H.; McCue, D.; Chapin, L. Increase light olefins production: New methods based on proven FCC technology provide additional olefins source. *Hydrocarb. Process.* **2004**, *83*, 61–66.
4. Grace Chan, K.; Inal, F.; Senkan, S. Suppression of coke formation in the steam cracking of alkanes: Ethane and propane. *Ind. Eng. Chem. Res.* **1998**, *37*, 901–907. [[CrossRef](#)]
5. Resasco, D.E.; Haller, G.L. Catalytic dehydrogenation of lower alkanes. In *Catalysis: Volume 11*; Spivey, J.J., Agarwal, S.K., Eds.; The Royal Society of Chemistry: London, UK, 1994; pp. 379–411.
6. Bañares, M.A. Supported metal oxide and other catalysts for ethane conversion: A review. *Catal. Today* **1999**, *51*, 319–348. [[CrossRef](#)]
7. Cavani, F.; Trifirò, F. The oxidative dehydrogenation of ethane and propane as an alternative way for the production of light olefins. *Catal. Today* **1995**, *24*, 307–313. [[CrossRef](#)]
8. Wang, S.; Murata, K.; Hayakawa, T.; Hamakawa, S.; Suzuki, K. Dehydrogenation of ethane with carbon dioxide over supported chromium oxide catalysts. *Appl. Catal. A* **2000**, *196*, 1–8. [[CrossRef](#)]
9. Li, Y.; He, X.; Wu, S.; Zhang, K.; Zhou, G.; Liu, J.; Zhen, K.; Wu, T.; Cheng, T. Cr-MCM-41 molecular sieves crystallized at room temperature for reaction of ethane with CO_2 . *J. Nat. Gas Chem.* **2005**, *14*, 207–212.
10. Wang, S.; Zhu, Z.H. Catalytic Conversion of Alkanes to Olefins by Carbon Dioxide Oxidative Dehydrogenation A Review. *Energy Fuel* **2004**, *18*, 1126–1139. [[CrossRef](#)]
11. Mimura, N.; Okamoto, M.; Yamashita, H.; Oyama, S.T.; Murata, K. Oxidative Dehydrogenation of Ethane over Cr/ZSM-5 Catalysts Using CO_2 as an Oxidant. *J. Phys. Chem. B* **2006**, *110*, 21764–21770. [[CrossRef](#)]
12. Cheng, Y.; Zhang, F.; Zhang, Y.; Miao, C.; Hua, W.; Yue, Y.; Gao, Z. Oxidative dehydrogenation of ethane with CO_2 over Cr supported on submicron ZSM-5 zeolite. *Chin. J. Catal.* **2015**, *36*, 1242–1248. [[CrossRef](#)]
13. Rahmani, F.; Haghighi, M.; Amini, M. The beneficial utilization of natural zeolite in preparation of Cr/clinoptilolite nanocatalyst used in CO_2 -oxidative dehydrogenation of ethane to ethylene. *J. Ind. Eng. Chem.* **2015**, *31*, 142–155. [[CrossRef](#)]
14. Rahmani, F.; Haghighi, M.; Mahboob, S. CO_2 -enhanced dehydrogenation of ethane over sonochemically synthesized Cr/clinoptilolite- ZrO_2 nanocatalyst: Effects of ultrasound irradiation and ZrO_2 loading on catalytic activity and stability. *Ultrason. Sonochem.* **2016**, *33*, 150–163. [[CrossRef](#)] [[PubMed](#)]
15. Michorczyk, P.; Pietrzyk, P.; Ogonowski, J. Preparation and characterization of SBA-1-supported chromium oxide catalysts for CO_2 assisted dehydrogenation of propane. *Microporous Mesoporous Mater.* **2012**, *161*, 56–66. [[CrossRef](#)]
16. Deng, S.; Li, H.; Li, S.; Zhang, Y. Activity and characterization of modified $\text{Cr}_2\text{O}_3/\text{ZrO}_2$ nano-composite catalysts for oxidative dehydrogenation of ethane to ethylene with CO_2 . *J. Mol. Catal. A Chem.* **2007**, *268*, 169–175. [[CrossRef](#)]
17. Asghari, E.; Haghighi, M.; Rahmani, F. CO_2 Oxidative Dehydrogenation of Ethane to Ethylene over Cr/MCM-41 Nanocatalyst Synthesized via Hydrothermal/Impregnation Methods: Influence of Chromium Content on Catalytic Properties and Performance. *J. Mol. Catal. A Chem.* **2016**, *418–419*, 115–124. [[CrossRef](#)]
18. Botavina, M.A.; Martra, G.; Agafonov, Y.A.; Gaidai, N.A.; Nekrasov, N.V.; Trushin, D.V.; Coluccia, S.; Lapidus, A.L. Oxidative dehydrogenation of C3–C4 paraffins in the presence of CO_2 over $\text{CrO}_x/\text{SiO}_2$ catalysts. *Appl. Catal. A* **2008**, *347*, 126–132. [[CrossRef](#)]
19. Michorczyk, P.; Ogonowski, J.; Niemczyk, M. Investigation of catalytic activity of CrSBA-1 materials obtained by direct method in the dehydrogenation of propane with CO_2 . *Appl. Catal. A* **2010**, *374*, 142–149. [[CrossRef](#)]

20. Józwiak, W.K.; Ignaczak, W.; Dominiak, D.; Maniecki, T.P. Thermal stability of bulk and silica supported chromium trioxide. *Appl. Catal. A* **2004**, *258*, 33–45. [[CrossRef](#)]
21. Liu, L.; Li, H.; Zhang, Y. Mesoporous silica-supported chromium catalyst: Characterization and excellent performance in dehydrogenation of propane to propylene with carbon dioxide. *Catal. Commun.* **2007**, *8*, 565–570. [[CrossRef](#)]
22. Michorczyk, P.; Ogonowski, J.; Kuśtrowski, P.; Chmielarz, L. Chromium oxide supported on MCM-41 as a highly active and selective catalyst for dehydrogenation of propane with CO₂. *Appl. Catal. A* **2008**, *349*, 62–69. [[CrossRef](#)]
23. Shi, X.; Ji, S.; Wang, K.; Li, C. Oxidative Dehydrogenation of Ethane with CO₂ over Novel Cr/SBA-15/Al₂O₃/FeCrAl Monolithic Catalysts. *Energy Fuel* **2008**, *22*, 3631–3638. [[CrossRef](#)]
24. Zhang, X.; Yue, Y.; Gao, Z. Chromium Oxide Supported on Mesoporous SBA-15 as Propane Dehydrogenation and Oxidative Dehydrogenation Catalysts. *Catal. Lett.* **2002**, *83*, 19–25. [[CrossRef](#)]
25. Wang, Y.; Ohishi, Y.; Shishido, T.; Zhang, Q.; Yang, W.; Guo, Q.; Wan, H.; Takehira, K. Characterizations and catalytic properties of Cr-MCM-41 prepared by direct hydrothermal synthesis and template-ion exchange. *J. Catal.* **2003**, *220*, 347–357. [[CrossRef](#)]
26. Takehira, K.; Ohishi, Y.; Shishido, T.; Kawabata, T.; Takaki, K.; Zhang, Q.; Wang, Y. Behavior of active sites on Cr-MCM-41 catalysts during the dehydrogenation of propane with CO₂. *J. Catal.* **2004**, *224*, 404–416. [[CrossRef](#)]
27. Al-Awadi, A.S.; El-Toni, A.M.; Alhoshan, M.; Khan, A.; Labis, J.P.; Al-Fatesh, A.; Abasaheed, A.E.; Al-Zahrani, S.M. Impact of precursor sequence of addition for one-pot synthesis of Cr-MCM-41 catalyst nanoparticles to enhance ethane oxidative dehydrogenation with carbon dioxide. *Ceram. Int.* **2019**, *45*, 1125–1134. [[CrossRef](#)]
28. Wu, R.; Xie, P.; Cheng, Y.; Yue, Y.; Gu, S.; Yang, W.; Miao, C.; Hua, W.; Gao, Z. Hydrothermally prepared Cr₂O₃-ZrO₂ as a novel efficient catalyst for dehydrogenation of propane with CO₂. *Catal. Commun.* **2013**, *39*, 20–23. [[CrossRef](#)]
29. Nakagawa, K.; Kajita, C.; Ide, Y.; Okamura, M.; Kato, S.; Kasuya, H.; Ikenaga, N.O.; Kobayashi, T.; Suzuki, T. Promoting effect of carbon dioxide on the dehydrogenation and aromatization of ethane over gallium-loaded catalysts. *Catal. Lett.* **2000**, *64*, 215–221. [[CrossRef](#)]
30. Nakagawa, K.; Kajita, C.; Okumura, K.; Ikenaga, N.-O.; Nishitani-Gamo, M.; Ando, T.; Kobayashi, T.; Suzuki, T. Role of Carbon Dioxide in the Dehydrogenation of Ethane over Gallium-Loaded Catalysts. *J. Catal.* **2001**, *203*, 87–93. [[CrossRef](#)]
31. Shen, Z.; Liu, J.; Xu, H.; Yue, Y.; Hua, W.; Shen, W. Dehydrogenation of ethane to ethylene over a highly efficient Ga₂O₃/HZSM-5 catalyst in the presence of CO₂. *Appl. Catal. A* **2009**, *356*, 148–153. [[CrossRef](#)]
32. Koirala, R.; Buechel, R.; Krumeich, F.; Pratsinis, S.E.; Baiker, A. Oxidative Dehydrogenation of Ethane with CO₂ over Flame-Made Ga-Loaded TiO₂. *ACS Catal.* **2015**, *5*, 690–702. [[CrossRef](#)]
33. Michorczyk, P.; Ogonowski, J. Dehydrogenation of propane to propene over gallium oxide in the presence of CO₂. *Appl. Catal. A* **2003**, *251*, 425–433. [[CrossRef](#)]
34. Li, H.; Yue, Y.; Miao, C.; Xie, Z.; Hua, W.; Gao, Z. Dehydrogenation of ethylbenzene and propane over Ga₂O₃-ZrO₂ catalysts in the presence of CO₂. *Catal. Commun.* **2007**, *8*, 1317–1322. [[CrossRef](#)]
35. Valenzuela, R.X.; Bueno, G.; Cortés Corberán, V.; Xu, Y.; Chen, C. Selective oxidehydrogenation of ethane with CO₂ over CeO₂-based catalysts. *Catal. Today* **2000**, *61*, 43–48. [[CrossRef](#)]
36. Valenzuela, R.X.; Bueno, G.; Solbes, A.; Sapiña, F.; Martínez, E.; Cortés Corberán, V. Nanostructured ceria-based catalysts for oxydehydrogenation of ethane with CO₂. *Top. Catal.* **2001**, *15*, 181–188. [[CrossRef](#)]
37. Zhang, X.; Ye, Q.; Xu, B.; He, D. Oxidative dehydrogenation of ethane over Co-BaCO₃ catalysts using CO₂ as oxidant: Effects of Co promoter. *Catal. Lett.* **2007**, *117*, 140–145. [[CrossRef](#)]
38. Elkabouss, K.; Kacimi, M.; Ziyad, M.; Ammar, S.; Bozon-Verduraz, F. Cobalt-exchanged hydroxyapatite catalysts: Magnetic studies, spectroscopic investigations, performance in 2-butanol and ethane oxidative dehydrogenations. *J. Catal.* **2004**, *226*, 16–24. [[CrossRef](#)]
39. Koirala, R.; Buechel, R.; Pratsinis, S.E.; Baiker, A. Silica is preferred over various single and mixed oxides as support for CO₂-assisted cobalt-catalyzed oxidative dehydrogenation of ethane. *Appl. Catal. A* **2016**, *527*, 96–108. [[CrossRef](#)]
40. Myint, M.; Yan, B.; Wan, J.; Zhao, S.; Chen, J.G. Reforming and oxidative dehydrogenation of ethane with CO₂ as a soft oxidant over bimetallic catalysts. *J. Catal.* **2016**, *343*, 168–177. [[CrossRef](#)]

41. Zhang, X.; Zhu, A.; Li, X.; Gong, W. Oxidative dehydrogenation of ethane with CO₂ over catalyst under pulse corona plasma. *Catal. Today* **2004**, *89*, 97–102. [[CrossRef](#)]
42. Peng, X.; Zhu, J.; Yao, L.; Hu, C. Effect of methane co-feeding on the selectivity of ethylene produced from oxidative dehydrogenation of ethane with CO₂ over a Ni-La/SiO₂ catalyst. *J. Energy Chem.* **2013**, *22*, 653–658. [[CrossRef](#)]
43. Xu, L.; Liu, J.; Yang, H.; Xu, Y.; Wang, Q.; Lin, L. Regeneration behaviors of Fe/SiO₂ and Fe–Mn/SiO₂ catalysts for C₂H₆ dehydrogenation with CO₂ to C₂H₄. *Catal. Lett.* **1999**, *62*, 185–189. [[CrossRef](#)]
44. Nakagawa, K.; Kajita, C.; Ikenaga, N.-o.; Nishitani-Gamo, M.; Ando, T.; Suzuki, T. Dehydrogenation of light alkanes over oxidized diamond-supported catalysts in the presence of carbon dioxide. *Catal. Today* **2003**, *84*, 149–157. [[CrossRef](#)]
45. Ogonowski, J.; Skrzyńska, E. Conversion of Lower Hydrocarbons in the Presence of Carbon Dioxide: The Theoretic Analysis and Catalytic Tests over Active Carbon Supported Vanadium Oxide. *Catal. Lett.* **2008**, *124*, 52–58. [[CrossRef](#)]
46. Qiao, A.; Kalevaru, V.N.; Radnik, J.; Martin, A. Oxidative dehydrogenation of ethane to ethylene over Ni–Nb–M–O catalysts: Effect of promoter metal and CO₂-admixture on the performance. *Catal. Today* **2016**, *264*, 144–151. [[CrossRef](#)]
47. Solymosi, F.; Németh, R. The oxidative dehydrogenation of ethane with CO₂ over Mo₂C/SiO₂ catalyst. *Catal. Lett.* **1999**, *62*, 197–200. [[CrossRef](#)]
48. Chen, M.; Xu, J.; Liu, Y.-M.; Cao, Y.; He, H.-Y.; Zhuang, J.-H. Supported indium oxide as novel efficient catalysts for dehydrogenation of propane with carbon dioxide. *Appl. Catal. A* **2010**, *377*, 35–41. [[CrossRef](#)]
49. Zhu, J.; Qin, S.; Ren, S.; Peng, X.; Tong, D.; Hu, C. Na₂WO₄/Mn/SiO₂ catalyst for oxidative dehydrogenation of ethane using CO₂ as oxidant. *Catal. Today* **2009**, *148*, 310–315. [[CrossRef](#)]
50. Wang, L.; Li, F.; Chen, Y.; Chen, J. Selective hydrogenation of acetylene on SiO₂-supported Ni–Ga alloy and intermetallic compound. *J. Energy Chem.* **2019**, *29*, 40–49. [[CrossRef](#)]
51. Clarke, J.K.A. Selectivity in catalysis by alloys. *Chem. Rev.* **1975**, *75*, 291–305. [[CrossRef](#)]
52. Bond, G.C. Supported metal catalysts: Some unsolved problems. *Chem. Soc. Rev.* **1991**, *20*, 441–475. [[CrossRef](#)]
53. Che, M.; Bennett, C.O. The Influence of Particle Size on the Catalytic Properties of Supported Metals. In *Advances in Catalysis*; Eley, D.D., Pines, H., Weisz, P.B., Eds.; Academic Press: Cambridge, MA, USA, 1989; Volume 36, pp. 55–172.
54. Pagán-Torres, Y.J.; Lu, J.; Nikolla, E.; Alba-Rubio, A.C. Chapter 17—Well-Defined Nanostructures for Catalysis by Atomic Layer Deposition. In *Studies in Surface Science and Catalysis*; Fornasiero, P., Cargnello, M., Eds.; Elsevier: Amsterdam, The Netherlands, 2017; Volume 177, pp. 643–676.
55. Jibril, B.Y.; Ahmed, S. Oxidative dehydrogenation of propane over Co, Ni and Mo mixed oxides/MCM-41 catalysts: Effects of intra- and extra-framework locations of metals on product distributions. *Catal. Commun.* **2006**, *7*, 990–996. [[CrossRef](#)]
56. Taghavinezhad, P.; Haghighi, M.; Alizadeh, R. Sonosynthesis of VO_x/MCM-41 nanocatalyst enhanced by various metal oxides (Mg, Al, Zr) for CO₂-oxidative dehydrogenation of ethane to ethylene. *Microporous Mesoporous Mater.* **2018**, *261*, 63–78. [[CrossRef](#)]
57. Le, L.; Yang, M.; Xiao, C.; Chen, A. Characterization and catalytic property of nano Cr-based catalysts for ethane dehydrogenation in CO₂. *Integr. Ferroelectr.* **2017**, *182*, 202–209. [[CrossRef](#)]
58. Shi, X.; Ji, S.; Wang, K. Oxidative Dehydrogenation of Ethane to Ethylene with Carbon dioxide over Cr–Ce/SBA-15 Catalysts. *Catal. Lett.* **2008**, *125*, 331–339. [[CrossRef](#)]
59. Burri, D.R.; Choi, K.-M.; Lee, J.-H.; Han, D.-S.; Park, S.-E. Influence of SBA-15 support on CeO₂–ZrO₂ catalyst for the dehydrogenation of ethylbenzene to styrene with CO₂. *Catal. Commun.* **2007**, *8*, 43–48. [[CrossRef](#)]
60. Wu, D.; Shen, R.; Yang, R.; Ji, W.; Jiang, M.; Ding, W.; Peng, L. Mixed Molybdenum Oxides with Superior Performances as an Advanced Anode Material for Lithium-Ion Batteries. *Sci. Rep.* **2017**, *7*, 44697. [[CrossRef](#)] [[PubMed](#)]
61. Dacquin, J.P.; Lee, A.F.; Pirez, C.; Wilson, K. Pore-expanded SBA-15 sulfonic acid silicas for biodiesel synthesis. *Chem. Commun.* **2012**, *48*, 212–214. [[CrossRef](#)] [[PubMed](#)]
62. Al-Awadi, A.S.; El-Toni, A.M.; Al-Zahrani, S.M.; Abasaeed, A.E.; Alhoshan, M.; Khan, A.; Labis, J.P.; Al-Fatesh, A. Role of TiO₂ nanoparticle modification of Cr/MCM41 catalyst to enhance Cr-support interaction for oxidative dehydrogenation of ethane with carbon dioxide. *Appl. Catal. A* **2019**, *584*, 117114. [[CrossRef](#)]

63. Arnoldy, P.; Franken, M.C.; Scheffer, B.; Moulijn, J.A. Temperature-programmed reduction of CoOMoO₃Al₂O₃ catalysts. *J. Catal.* **1985**, *96*, 381–395. [[CrossRef](#)]
64. Solsona, B.; Blasco, T.; López Nieto, J.M.; Peña, M.L.; Rey, F.; Vidal-Moya, A. Vanadium Oxide Supported on Mesoporous MCM-41 as Selective Catalysts in the Oxidative Dehydrogenation of Alkanes. *J. Catal.* **2001**, *203*, 443–452. [[CrossRef](#)]
65. De Rossi, S.; Pia Casaletto, M.; Ferraris, G.; Cimino, A.; Minelli, G. Chromia/zirconia catalysts with Cr content exceeding the monolayer. A comparison with chromia/alumina and chromia/silica for isobutane dehydrogenation. *Appl. Catal. A* **1998**, *167*, 257–270. [[CrossRef](#)]
66. Zhao, X.; Wang, X. Synthesis, characterization and catalytic application of Cr-SBA-1 mesoporous molecular sieves. *J. Mol. Catal. A Chem.* **2007**, *261*, 225–231. [[CrossRef](#)]
67. Weckhuysen, B.M.; Verberckmoes, A.A.; Debaere, J.; Ooms, K.; Langhans, I.; Schoonheydt, R.A. In situ UV-Vis diffuse reflectance spectroscopy—On line activity measurements of supported chromium oxide catalysts: Relating isobutane dehydrogenation activity with Cr-speciation via experimental design. *J. Mol. Catal. A Chem.* **2000**, *151*, 115–131. [[CrossRef](#)]
68. Weckhuysen, B.M.; Wachs, I.E.; Schoonheydt, R.A. Surface Chemistry and Spectroscopy of Chromium in Inorganic Oxides. *Chem. Rev.* **1996**, *96*, 3327–3350. [[CrossRef](#)] [[PubMed](#)]
69. Weckhuysen, B.M.; Verberckmoes, A.A.; Baets, A.R.D.; Schoonheydt, R.A. Diffuse Reflectance Spectroscopy of Supported Chromium Oxide Catalysts: A Self-Modeling Mixture Analysis. *J. Catal.* **1997**, *166*, 160–171. [[CrossRef](#)]
70. Ayari, F.; Mhamdi, M.; Álvarez-Rodríguez, J.; Ruiz, A.R.G.; Delahay, G.; Ghorbel, A. Selective catalytic reduction of NO with NH₃ over Cr-ZSM-5 catalysts: General characterization and catalysts screening. *Appl. Catal. B Environ.* **2013**, *134–135*, 367–380. [[CrossRef](#)]
71. Michorczyk, P.; Ogonowski, J.; Zeńczak, K. Activity of chromium oxide deposited on different silica supports in the dehydrogenation of propane with CO₂—A comparative study. *J. Mol. Catal. A Chem.* **2011**, *349*, 1–12. [[CrossRef](#)]
72. Cavani, F.; Koutyrev, M.; Trifirò, F.; Bartolini, A.; Ghisletti, D.; Iezzi, R.; Santucci, A.; Del Piero, G. Chemical and Physical Characterization of Alumina-Supported Chromia-Based Catalysts and Their Activity in Dehydrogenation of Isobutane. *J. Catal.* **1996**, *158*, 236–250. [[CrossRef](#)]
73. Puurunen, R.L.; Weckhuysen, B.M. Spectroscopic Study on the Irreversible Deactivation of Chromia/Alumina Dehydrogenation Catalysts. *J. Catal.* **2002**, *210*, 418–430. [[CrossRef](#)]
74. Hakuli, A.; Harlin, M.E.; Backman, L.B.; Krause, A.O.I. Dehydrogenation of i-Butane on CrO_x/SiO₂ Catalysts. *J. Catal.* **1999**, *184*, 349–356. [[CrossRef](#)]
75. Wang, G.; Zhang, L.; Deng, J.; Dai, H.; He, H.; Au, C.T. Preparation, characterization, and catalytic activity of chromia supported on SBA-15 for the oxidative dehydrogenation of isobutane. *Appl. Catal. A* **2009**, *355*, 192–201. [[CrossRef](#)]
76. Kim, D.S.; Tatibouet, J.-M.; Wachs, I.E. Surface structure and reactivity of CrO₃/SiO₂ catalysts. *J. Catal.* **1992**, *136*, 209–221. [[CrossRef](#)]
77. Ge, X.; Zhu, M.; Shen, J. Catalytic performance of silica-supported chromium oxide catalysts in ethane dehydrogenation with carbon dioxide. *React. Kinet. Catal. Lett.* **2002**, *77*, 103–108. [[CrossRef](#)]
78. Sharma, S.; Hilaire, S.; Vohs, J.M.; Gorte, R.J.; Jen, H.W. Evidence for Oxidation of Ceria by CO₂. *J. Catal.* **2000**, *190*, 199–204. [[CrossRef](#)]
79. Blasco, T.; Galli, A.; López Nieto, J.M.; Trifirò, F. Oxidative Dehydrogenation of Ethane and n-Butane on VO_x/Al₂O₃ Catalysts. *J. Catal.* **1997**, *169*, 203–211. [[CrossRef](#)]
80. Nieto, J.L.; Soler, J.; Concepción, P.; Herguido, J.; Menéndez, M.; Santamaría, J. Oxidative dehydrogenation of alkanes over V-based catalysts: Influence of redox properties on catalytic performance. *J. Catal.* **1999**, *185*, 324–332. [[CrossRef](#)]
81. Pacheco, M.L.; Soler, J.; Dejoz, A.; López Nieto, J.M.; Herguido, J.; Menéndez, M.; Santamaría, J. MoO₃/MgO as a catalyst in the oxidative dehydrogenation of n-butane in a two-zone fluidized bed reactor. *Catal. Today* **2000**, *61*, 101–107. [[CrossRef](#)]

